Optics & Laser Technology 168 (2024) 109886

Contents lists available at ScienceDirect

Optics and Laser Technology

journal homepage: www.elsevier.com/locate/optlastec

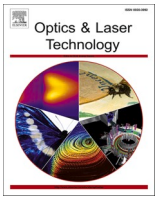

Full length article

Preparation of uniform Ag nanoparticles with enhanced plasmon resonance intensity and antibacterial efficiency via two-step dewetting process

Jyun-Jhih Wang [a], I-Chia Chen [b], Hsuan-Kai Lin [b,*], Yu-Chung Lin [a], Chien-Jung Huang [a]

[a] Department of Laser Micro-processing Technology, Industrial Technology Research Institute Southern Region Campus, Tainan, Taiwan
[b] Department of Materials Engineering, National Pingtung University of Science and Technology, Pingtung, Taiwan

ARTICLE INFO

Keywords:
Two-step dewetting
Laser
Surface plasmon resonance
Escherichia coli

ABSTRACT

Ag thin films were deposited on glass substrates by a high vacuum sputtering system. The films were then processed by three different dewetting methods: thermal aging, pulse-laser irradiation, and two-step dewetting (thermal aging and laser irradiation). The morphologies, crystalline structures, optical properties, Raman signal intensity, and antibacterial efficiency of the dewetted Ag films were analyzed and compared. The island structures of the as-sputtered Ag film were transformed into nanoparticles as the annealing temperature increased. Furthermore, the nanoparticle size decreased with an increasing laser energy. The two-step dewetting process resulted in the formation of small nanoparticles with a narrow size distribution and a strong SPR intensity. A strong Raman peak was also observed for a 1000 ppm melamine aqueous solution deposited on the dewetted surface. The two-step dewetted film showed a better antibacterial efficiency against *Escherichia coli*, *Staphylococcus aureus* and *Pseudomonas aeruginosa* bacteria than the films processed by thermal aging or laser dewetting alone. Moreover, the two-step dewetted Ag film induced a greater ROS generation rate after contact with the *Escherichia coli*, *Staphylococcus aureus* and *Pseudomonas aeruginosa* bacteria for 24 hr. The greater antibacterial efficiency and Raman signal intensity of the two-step dewetted film were both attributed to the effect of the small nanoparticles in increasing the contact area between the dewetted surface and the bacteria or melamine solution, respectively. Overall, the two-step dewetting process appears to be a promising approach for the fabrication of uniform small-sized nanoparticles for a wide range of applications.

1. Introduction

Nanoparticles (NPs) are widely used in many fields nowadays, including optoelectronics [1], biomedicine [2,3], anti-microorganisms [4,5], and Raman detection [6,7]. Noble metal NPs (e.g., Au, Ag, and Cu) have attracted particular attention due to their strong surface plasmon resonance (SPR) effect and excellent electric field properties [8]. The superior SPR properties of such NPs are due to their element composition, size, and shape, and are also strongly affected by the local dielectric environment [9,10]. Noble metal NPs enhance the heat spot effect in surface enhanced Raman spectroscopy (SERS), and are therefore extensively used in medical diagnosis [11], plant pathogen detection [7], and food safety monitoring [12].

NPs can be produced by many methods, including chemical [13], hydrothermal [14], methanol catalysis [15] and laser dewetting [4,5,16–18]. However, metal NPs produced by chemical techniques typically show a poor adhesion to the substrate. Furthermore, the NPs prepared using hydrothermal or methanol catalysis methods suffer the disadvantages of incomplete crystal growth information [19]. Accordingly, the use of dewetting techniques to induce small particles or nanostructures on the substrate surface has attracted growing attention in recent years [16,20]. The dewetting mechanism exploits the natural tendency of thin films to minimize the interfacial energy or free surface energy when exposed to heating [16,20]. General physical dewetting methods are time consuming and result in a non-uniform distribution of the NP size [20]. However, laser dewetting, with its advantage of a strong local heating effect, provides a simple, convenient and low-cost approach for forming NPs with properties governed by the laser parameters [4,5,18].

The following controlled-dewetting approaches for metallic nanostructuring can be found in these literatures: (1) dewetting of films on pre-patterned substrates [21,22], (2) dewetting of template-confined film [23,24], and (3) dewetting driven by nanoscale Rayleigh-Taylor instability [25–27]. Moreover, the characteristics of silver

* Correspondent author.
E-mail address: HKLin@mail.npust.edu.tw (H.-K. Lin).

https://doi.org/10.1016/j.optlastec.2023.109886
Received 25 February 2023; Received in revised form 30 June 2023; Accepted 27 July 2023

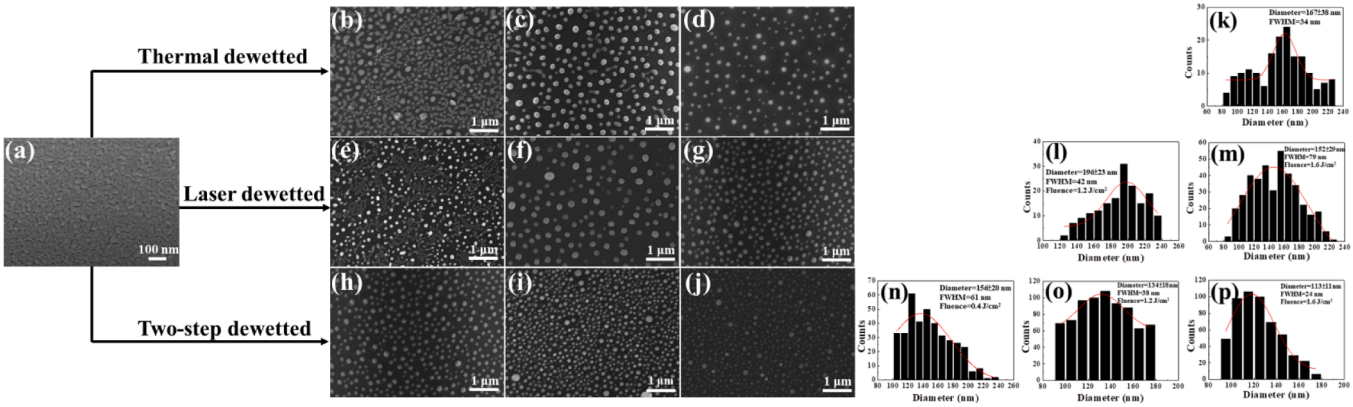

Fig. 1. (a) SEM image of 10-nm Ag film deposited on glass; (b, c, d) thermal dewetted Ag films with holding time of 2 min and holding temperatures of 200, 300, and 400°; (k) corresponding size distribution of NPs; (e, f, g) laser dewetted Ag films with repetition rate of 400 kHz, scanning speed of 400 mm/s, and laser powers of 2, 6, and 8 W (fluence were 0.4, 1.2 and 1.6 J/cm^2), respectively; (l-m) corresponding size distributions of NPs; (h, i, j) two-step dewetted Ag films (thermal dewetting at 200 °C for 2 min followed by laser irradiation with parameters of 400 kHz; 400 mm/s; 2, 6, and 8 W (fluence were 0.4, 1.2 and 1.6 J/cm^2), respectively; (n-p) corresponding size distributions of NPs.

nanostructures created by pulsed laser annealing in the air and an additional heating up to a temperature of 220 °C was implemented to avoid thermomechanical stresses during laser exposure [28]. While the dewetting of single-layer thin silver films using nanosecond pulsed laser irradiation has been reported to make Ag NPs on various substrates of quartz [29], glass [30–32], mica [33], and SiO_2 [34]. Moreover, previous research in recent year has shown that laser dewetting process can apply to various fields due to their adjustable and resilient process such as biomedical [4,5], Raman detection [6], surface plasma resonance behaviors [18]. It showed the potential for developing the laser dewetting technique and used for different areas. Some studies have suggested the mechanisms and methods of dewetting process. However, the two-step dewetting process and the different density of Ag NPs distribution against antibacterial affect and Raman detection was rarely studied.

Therefore, the present study prepares NPs in Ag thin films deposited on glass substrates using three different dewetting processes, namely thermal aging, pulse-laser irradiation, and two-step thermal aging followed by laser irradiation. The microstructures, size distributions, optical properties, and crystalline characteristics of the NPs formed using the three different methods are investigated and compared. The Ag NPs induced by the two-step dewetting process are then applied for melamine detection and antibacterial activity tests, respectively. In general, the results show that the Ag NPs have a narrow-size distribution with excellent SPR, Raman, and antibacterial properties.

2. Materials and methods

Glass (CK) substrates with a thickness of 0.7 mm and transmittance of 90% at a wavelength of 550 nm were purchased from ruilong company, Taiwan. The substrates were cleaned in acetone, ethanol, and deionized water for 5 mins and then dried in air. 10-nm thickness Ag thin films were deposited on the glass substrates by a high vacuum sputtering system (KD-SPUTTER + LL, Kao Duen Co., Ltd, Taiwan). The microstructures of the as-sputtered films were examined by an X-ray Diffractometer (D8, Bruker, USA) with Cu-Kα radiation (λ = 0.154 nm). Thermal dewetting was performed in an RTA furnace with an Ar atmosphere at temperatures of 200, 300, and 400 °C, respectively, and a holding time of 2 min in each case. Consequently, laser dewetting was performed using a pulsed NIR fiber laser system (G3-SM, UK) with a wavelength of 1064 nm and the spot size of 40 μm. The irradiation process was performed using a high repetition rate of 400 kHz, a scanning speed of 400 mm/s, and laser powers of 2, 6 and 8 W, respectively. Finally, the two-step dewetting process was performed by aging the as-sputtered film at 200 °C for 2 min and then irradiating the film using a laser repetition rate of 400 kHz, a scanning speed of 400 mm/s, and laser powers of 2, 6, and 8 W, respectively. The following overlap percentage can be defined:

$$\text{Overlap}\,(\%) = \left(1 - \frac{\frac{v}{f}}{D + vt}\right) \times 100 \tag{1}$$

where v is the scan speed, D is the diameter of the laser spot (40 μm), and t is the pulse width (200 ns).

The overlap percentage can be acquired by Eq. (1) and it is 98%.

The fluence of the laser is given by.

$$\text{Fluence}\,(\text{J/cm2}) = \frac{\frac{P}{f}}{\pi r^2} \tag{2}$$

where P is laser power (W), f is the repetition rate (Hz) and r is the radius of the laser spot (20 μm). The fluence are 0.4, 1.2 and 1.6 J/cm^2 for 2, 6 and 8 W, respectively.

The NPs size and amount of captured images were quantified by the ImageJ software (National Institutes of Health, USA). The absorption properties of the as-sputtered film and dewetted Ag films were measured by a spectrophotometer (Lambda 35, U.S.A). The wettability of the films was measured by a contact angle system (OCA 15EC, Germany). The feasibility of the dewetted Ag films for Raman detection was investigated using an aqueous melamine solution with a concentration of 1000 ppm. The Raman spectra of the melamine solution on the various dewetted Ag films were measured by a Micro Raman system with a wavelength of 532 nm (MRI532S, Taiwan). *Escherichia coli* (ATCC23815), *Staphylococcus aureus* and *Pseudomonas aeruginosa* were cultured in lysogeny broth at 37 °C and agitated at 150 rpm for 8 h. The cultured bacteria were then seeded on blank glass slides and dewetted Ag films with a concentration of 10^5 ml/colony-forming units (CFUs) and incubated at 37 °C for 24 h under 100% relative humidity (RH) conditions. The resulting solutions were diluted, plated on nutrient agar (NA) and incubated at 37 °C for a further 8 h. The CFUs were then counted. Finally, the reactive oxygen species (ROS) generation rate of the as-sputtered and dewetted Ag films was evaluated by staining with H_2DCFDA for 20 min and then performing fluorescence microscopy observations.

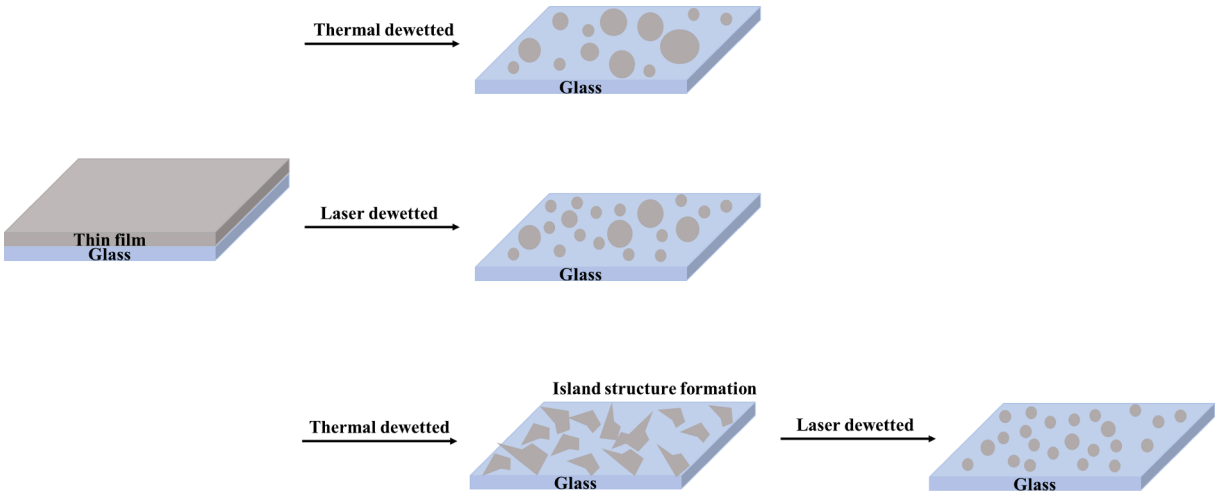

Fig. 2. Dewetting mechanisms of different Ag NP fabrication methods.

3. Results and discussions

3.1. Effects of thermal, laser and two-step dewetting process on surface morphology and NP formation

Fig. 1(a) shows the surface morphology of the as-sputtered 10-nm Ag film. Fig. 1(b)-(d) show the morphologies of the dewetted films annealed at temperatures of 200, 300, and 400 °C for two minutes, respectively. For annealing temperatures of 200 and 300 °C, the energy input is insufficient to dewet the Ag film completely, and hence island-like structures are formed. For a higher temperature of 400 °C, NPs are produced. However, they have an uneven size distribution. Fig. 1(e)-(g) show the surface morphologies of the Ag films processed by pulse-laser irradiation with a repetition rate of 400 kHz, a scanning speed of 400 mm/s, and laser pulse powers of 2, 6, and 8 W, respectively. For a laser power of 2 W (Fig. 1(e)), island structures are formed since the input energy is insufficient to form NPs. However, for higher laser powers of 6 and 8 W (Fig. 1(f)-(g)), the film is fully dewetted into NPs. The results are thus consistent with those of previous studies which showed that NPs are only formed once the laser pulse energy exceeds a certain critical threshold [16,18,20]. Fig. 1(h)-(j) show the surface morphologies of the Ag films thermally dewetted at 200 °C for 2 min and then irradiated with a repetition rate of 400 kHz, a scanning speed of 400 mm/s, and laser pulse powers of 2, 6, and 8 W, respectively. It is seen that NPs are formed in every case and have a uniform and smaller size than those produced in the thermal aging and laser irradiation dewetting processes. Fig. 1(k-p)) show the size distributions of the NPs produced in the Ag films processed using the various dewetting methods (thermal, laser, two-step dewetting). For all of the films, the particle size has a normal distribution with a range of 90 ~ 240 nm. For the thermally-aged (Fig. 1(k)) and laser-irradiated, (Fig. 1(l-m)) films, the particles have a relatively broad size distribution. Moreover, in the case of the laser dewetted film, the mean particle size reduces with an increasing laser power. For the two-step dewetting process (Fig. 1(n-p)), the particles have a narrow size distribution and the minimum mean particle size is obtained for a laser power of 8 W.

Fig. 2 shows the effects of the various dewetting mechanisms on the formation of Ag NPs in the Ag film. In general, dewetting involves the rupture of a thin liquid film on a substrate and the subsequent formation of droplets or NPs [20]. Dewetting is induced by atomic diffusion and can be driven by either minimum surface energy or minimum interface energy [16,18,20]. Typically, the dewetting efficiency is reduced in metallic thin films with a large atomic volume, and the resulting NPs tend to have a larger size and a lower density. For the present Ag thin films processed by thermal dewetting, island structures are formed at the edge of the film as the annealing temperature increases from 200 to 300 °C due to the aggregation of the Ag atoms. These island structures then transform to NPs as the temperature further increases to 400 °C. Solid-state dewetting of thin metallic films deposited on an inert substrate is considered as a simple method for the fabrication of metal

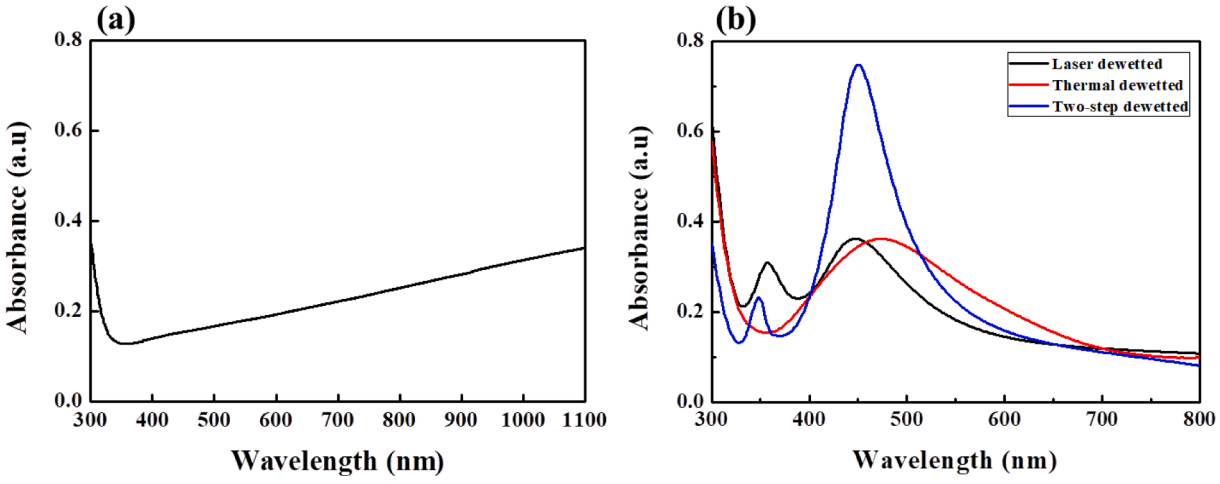

Fig. 3. Absorption spectra of: (a) as-sputtered 10-nm Ag film, and (b) dewetted Ag films.

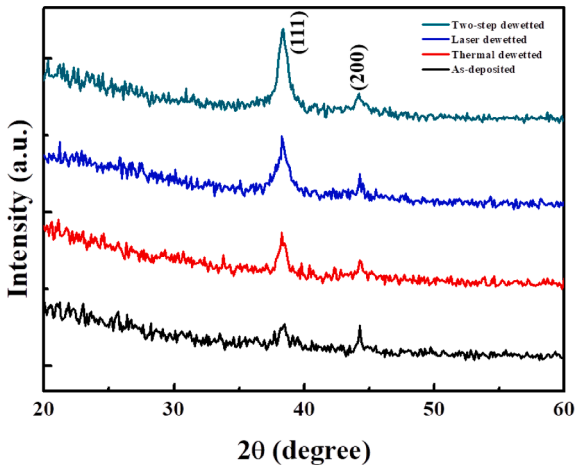

Fig. 4. XRD patterns of as-deposited Ag film and dewetted Ag films.

nanoparticles [22]. It occurs via diffusion even in the solid state at the temperature well below the melting point (961 °C) of the Ag films. For the Ag film treated by pulse-laser irradiation, the film first transforms into island structures under a low irradiation power, and these structures then further transform to small particles with a broad size distribution as the laser power increases. For both films, NP formation commences from the island structures rather than the continuous as-sputtered film. Thus, in the proposed two-step dewetting process, the Ag film was pre-annealed in order to create island structures, and laser irradiation was then performed to generate NPs with a narrow size particle size distribution.

3.2. Optical absorption properties of dewetted Ag films

Fig. 3(a) shows the absorption spectrum of the as-deposited Ag film. The absorption intensity of 10 nm Ag thin film in the wavelength of 1064 nm was 0.33 a.u (Fig. 3 (a)). No absorption peak is observed since the energy input during the sputtering process is insufficient to induce NPs (Fig. 1(a)). Fig. 3(b) presents the absorption spectra for the three dewetted Ag films. All the films show a strong SPR peak in the range of 400–500 nm. The results are thus consistent with those of a previous study which also showed a strong absorption peak for Ag films at wavelengths of 400–500 nm [16]. Fig. 3(b) shows that the absorption spectrum reveal that the SPR peak can also be found at wavelengths of 350–370 nm in laser dewetting and two-step dewetting process. The NPs are uniform across the particle electromagnetic field that produce the primary dipole-type oscillation SPR peak. On the other hand, the phase delay excites higher multipolar resonance, lead to several SPR peaks in the spectrum [35,36]. In general, SPR occurs when the NP size is less than the wavelength of the incident light [37]. The NPs formed in the present thermal dewetted film (Fig. 1(d)) and laser dewetted film (Fig. 1 (g)) have a size of 167 ± 38 nm and 152 ± 29 nm, respectively. By contrast, the NPs in the two-step dewetted Ag film (Fig. 1 (j)) have a size of just 113 ± 11 nm. Thus, the two-step dewetted film exhibits a stronger SPR peak than the other two dewetted films due to the small nanoparticle size and narrow size distribution. Moreover, the SPR peaks of the laser dewetted and two-step dewetted Ag films exhibit a blue shift due to the small NP size. By contrast, the SPR peak of the thermal dewetted film shows a red shift due to the large NP size, which results in a non-uniform distribution of the electric field of the incident light around the particles [5,18]. Overall, the results indicate that the three dewetting techniques provide the ability to adjust both the position and the intensity of the SPR peak.

3.3. Structures of dewetted Ag films and melamine Raman detection

Fig. 4(a) shows the XRD patterns of the as-sputtered and dewetted films. It is seen that the dewetting process results in a crystallization of the Ag film due to heat energy input during the aging and/or laser irradiation process. Of the three dewetted films, the two-step dewetted film shows the most intense diffraction peaks due to the small and narrow-size distribution of the NPs. Fig. 5(a) shows the Raman spectra obtained for aqueous melamine solutions with a concentration of 1000 ppm deposited on the as-sputtered and dewetted Ag films. The excitation wavelength is 532 nm in every case. A characteristic peak is observed at 676–680 cm^{-1} in all of the spectra. The results are therefore consistent with the finding of a previous study [6] that melamine shows a pronounced peak in the Raman spectrum at 676 cm^{-1}. It is additionally seen that the two-step dewetting process results in a stronger Raman signal than either the thermal aging treatment or the laser irradiation treatment. As described above, the uniform NP size and narrow particle size distribution in the two-step dewetted film result in a more intensive plasmon resonance effect. Fig. 5(b) shows the relationship between the SPR intensity and the Raman intensity for the four Ag films. A positive correlation is observed between the two intensity signals. Thus, a strong SPR intensity is associated with a strong Raman signal intensity. Consequently, the two-step dewetted Ag film shows the strongest Raman signal intensity (1658 a.u) among the various films (as-sputtered film: 441 a.u; thermal dewetted film: 533 a.u; and laser dewetted film: 1322 a.u). Fig. 5(c) shows relation of the diverse dewetting process between the SPR position and the full width at half maximum, FWHM of the three dewetted Ag films. Compare to thermal and laser dewtted Ag film, the two-step dewetted Ag film displays the blue shift of SPR position due to the smaller NPs size. In addition, the two-step dewetted Ag film has the narrower FWHM of 62 nm than thermal aging (176 nm) and laser irradiation (77 nm) because of the even NPs distribution. For the latter three films, the non-uniform particle distribution results in an inhomogeneous electric field, and hence the SPR / Raman response is suppressed [9]. By contrast, the uniform small-size particle distribution in the two-step dewetted film improves the uniformity of the electromagnetic field and increases the intensity of the SPR / Raman signal

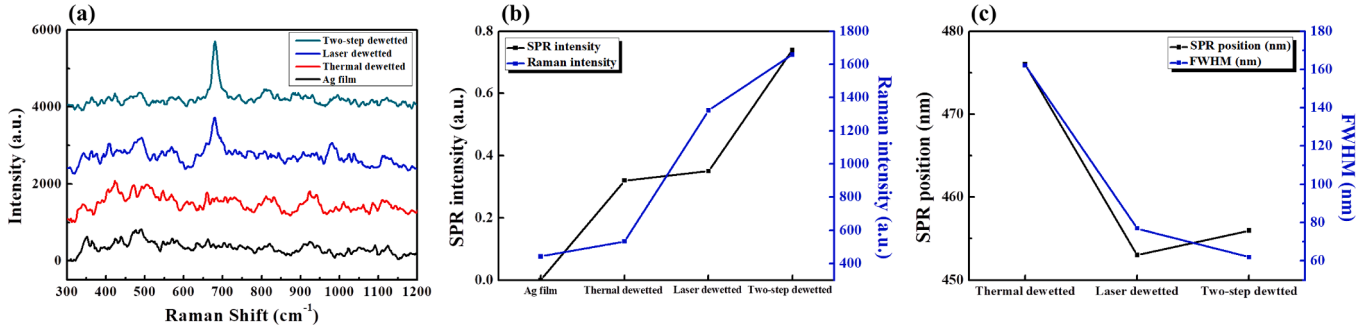

Fig. 5. (a) Raman spectra for 1000 ppm melamine solution on as-sputtered Ag film and dewetted Ag films; (b) relationship between SPR intensity and Raman intensity for as-sputtered Ag film and dewetted Ag films; (c) relationship between SPR position and FWHM for various dewetted Ag films.

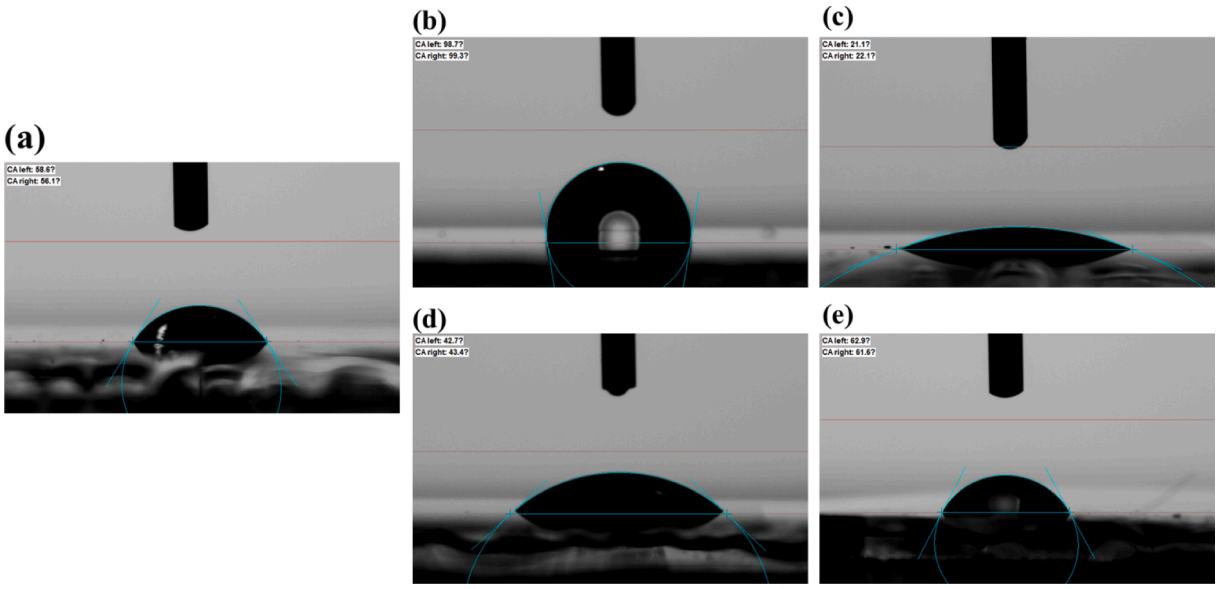

Fig. 6. Contact angle images for various surfaces: (a) bare glass substrate (CK), (b) as-sputtered Ag film, (c) thermal dewetted Ag film, (d) laser dewetted Ag film, and (e) two-step dewetted Ag film.

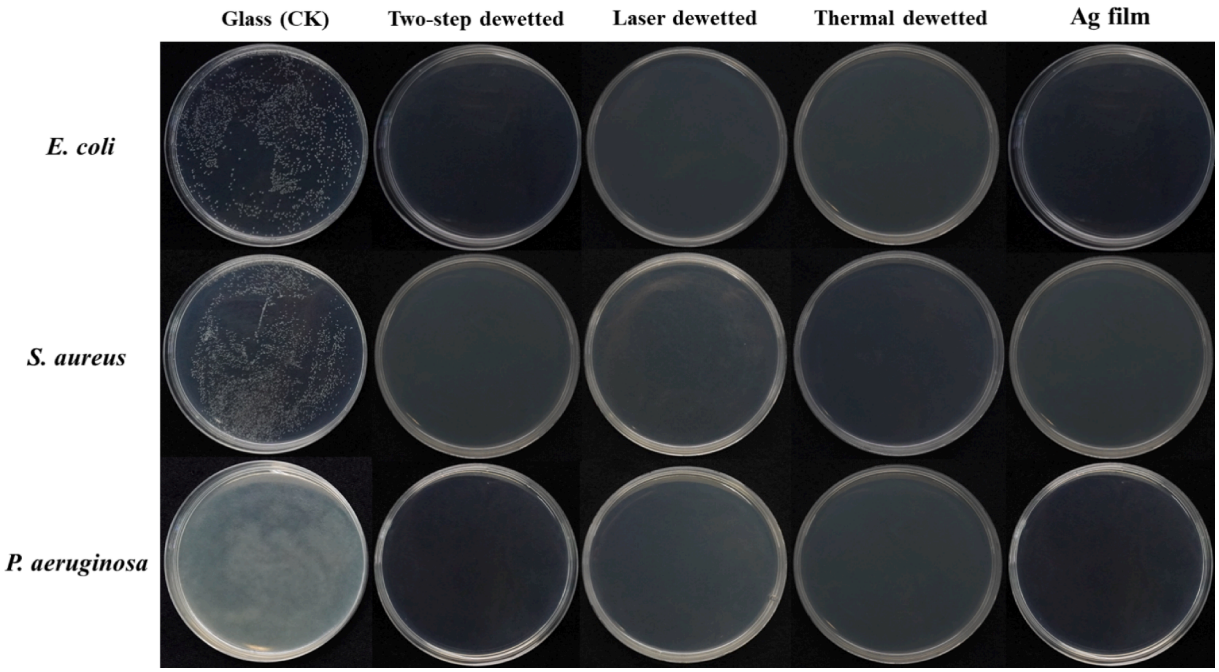

Fig. 7. Antibacterial effects of glass, dewetted Ag films, and as-sputtered Ag film against *Escherichia coli*, *Staphylococcus aureus* and *Pseudomonas aeruginosa* after 24 h exposure.

accordingly. In the SERS process, the relative position of the sample to the hot spot has a strong effect on the enhancement performance, and only the molecules located at the hot spot are significantly enhanced [38]. The SERS hotspot is determined mainly by the excitation wavelength and shape and size of the NPs [38,39]. In other words, the shape, size, and size distribution of the particles are key factors in determining the intensity of the Raman signal. Hence, the two-step dewetted film shows the strongest SPR / Raman intensity and the sharpest peak of the various films since the small and uniform particle size enhances the electromagnetic field and resonance quality.

3.4. Wettability and antibacterial activity of dewetted films

Fig. 6 shows contact angle images of the as-sputtered and dewetted films. As shown in Fig. 6(a), the original glass slide has a contact angle of 57°. The contact angle of the as-sputtered Ag film increases to 98° as a result of the smooth surface (Fig. 6 (b)). The contact angle reduces to 21° for the thermal dewetted film (Fig. 6(c)). However, it then increases to 42° (Fig. 6(d)) and 62° (Fig. 6(e)) for the laser dewetted and two-step dewetted films, respectively. The greater contact angle in the latter two cases is the result of an increased particle uniformity and reduced particle size, which increase the particle density and thus provide a better support of the droplet structure. The surface conditions are a key factor in determining the antimicrobial effect. In particular,

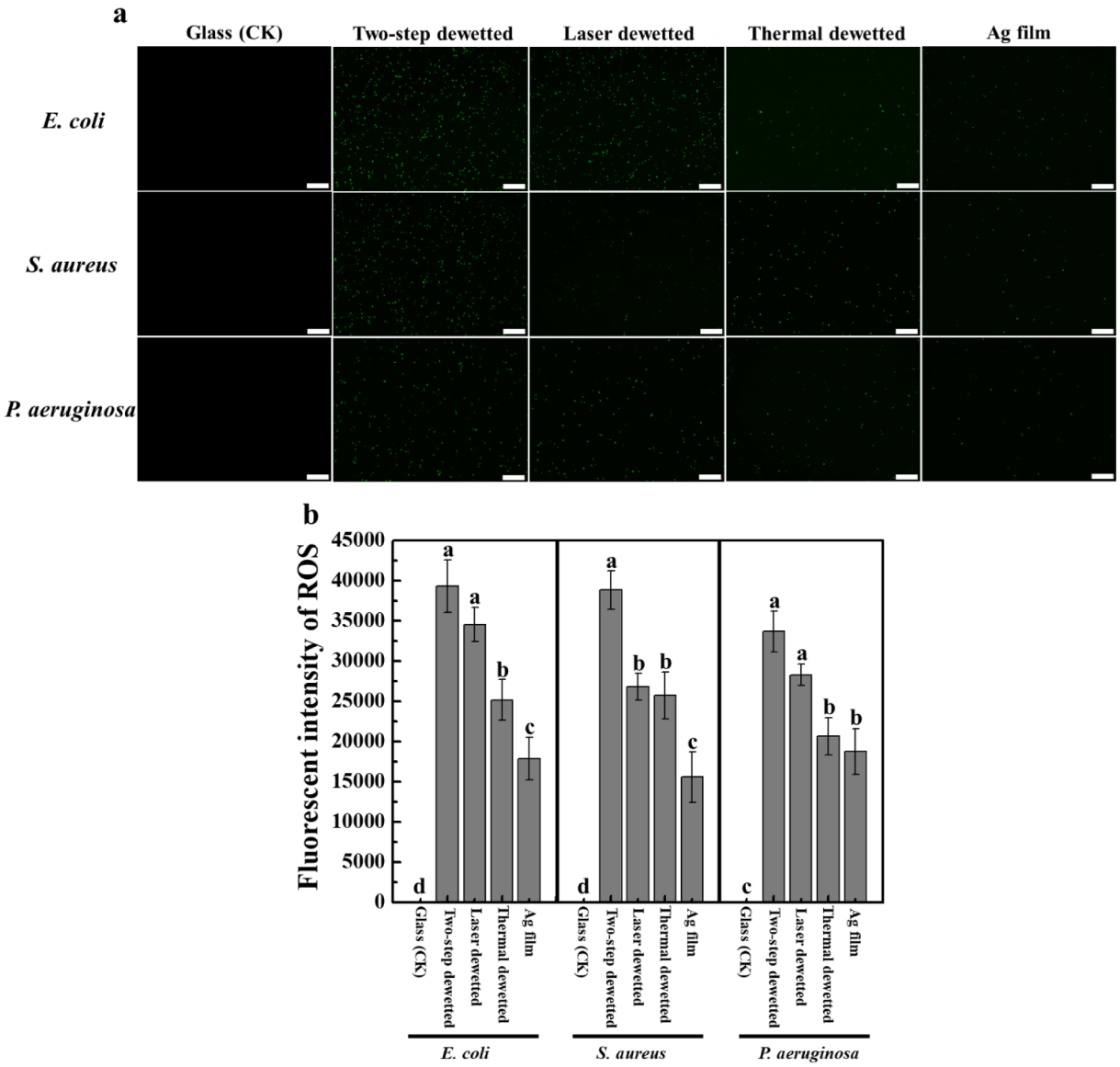

Fig. 8. Effects of various surfaces on ROS generation for *Escherichia coli*, *Staphylococcus aureus* and *Pseudomonas aeruginosa* after exposure for 24 hr. (a) Fluorescence images showing ROS generation on glass (CK), dewetted Ag films, and as-sputtered Ag film. Note that the scale bars indicate a length of 20 μm. (b) Fluorescent intensity of ROS as determined by ImageJ image-processing software. Note that the letters (a, b, c and d) indicate significant differences according to Tukey's HSD test ($P < 0.05$).

microorganisms have difficulty attaching to (or moving on) hydrophobic surfaces [2,3]. Fig. 7 shows the antibacterial activities of the glass slide and various dewetted Ag films against *Escherichia coli*, *Staphylococcus aureus* and *Pseudomonas aeruginosa*, respectively. It is seen that a large number of bacteria exist on the glass (CK) slide after 24 h for all three cases. However, no significant CFUs are detected on either the as-sputtered Ag film or the dewetted Ag films. In other words, the Ag film and dewetted Ag films have a 100% antibacterial efficiency for all three bacteria (both gram-negative and gram-positive). The reactive oxygen species (ROS) generation rates of the various surfaces were tested after an incubation time of 24 h using H_2DCFDA fluorescent probe. Fig. 8(a) shows the corresponding fluorescence images, where the ROS is manifested as green fluorescence. The images confirm that no ROS is generated on the glass slide for any of the bacteria. By contrast, significant ROS generation is observed for both the as-sputtered Ag film and the dewetted Ag films.

Fig. 8(b) shows the ROS fluorescent intensities of the glass slide and various Ag films. The ROS generation rate of the laser dewetted Ag film is greater than that of the thermal dewetted film. Moreover, the ROS generation rate of the two-step dewetted film is greater than that of the laser dewetted film since the small and uniform-sized NPs result in a greater contact area with the bacteria. It was shown in [3] that metal NPs provide an effective alternative to fungicides for the sterilization of medical devices since the nanostructures increase the contact area of the surface and promote a fuller interaction with the microorganisms as a result [40,41]. Many recent studies have shown that metal particles such as silver (Ag), copper (Cu), gold (Au) and zinc (Zn) have a good antibacterial activity [3–5,42,43] since they readily interact with the respiratory enzymes attached to the cell membrane, induce free radical formation (ROS), and release metal ions [5,44]. The released ions then prompt membrane dysfunction, which leads to the eventual death of the bacteria [5,42,45].

4. Conclusions

This study has examined the effects of three dewetting processes (thermal annealing, pulse-laser irradiation, and two-step dewetting (thermal annealing followed by laser irradiation) in inducing the

formation of NPs in sputtered Ag thin films. For the thermal dewetted films, the NPs were formed only at a high temperature and had a non-uniform size in the range of 92 to 236 nm. For the laser dewetted films, NPs with a size of 96 to 221 nm were induced at higher laser powers of 6 and 8 W, respectively, and the particle size reduced with an increasing laser power. Finally, for the two-step dewetting process, uniform and small-sized NPs with a size of 102 to 201 nm were formed for all values of the laser power (4, 6 and 8 W). The uniform and narrow-size distribution of the NPs in the two-step dewetted film enhanced the SPR peak signal intensity and resulted in a blue shift of the absorbance spectrum. The two-step dewetted film similarly showed the strongest Raman intensity among all the dewetted films for 1000 pm aqueous melamine solutions. All three dewetted Ag films showed an antibacterial efficiency of 100% against *Escherichia coli*, *Staphylococcus aureus* and *Pseudomonas aeruginosa* bacteria following contact for 24 h. However, the ROS generation of the two-step dewetted film was significantly greater than that of the laser irradiated film and thermal aged film. In conclusion, the two-step dewetting process employed in the present study results in the formation of uniform NPs with a small size and a narrow size distribution. The NPs provide a strong antibacterial performance due to their effect in increasing the contact area between the dewetted surface and the microorganisms. They also result in an enhanced Raman signal intensity for melamine. Thus, this study defines the relationship of Ag NPs uniformity between antibacterial efficiency and Raman signal intensity and provides the adjustable and scalable method of forming Ag NPs array. The two-step dewetting process appears to provide a promising approach for the formation of uniform metal NPs for a wide range of applications in the medical, sensing, and optical absorbance fields.

Declaration of Competing Interest

The authors declare that they have no known competing financial interests or personal relationships that could have appeared to influence the work reported in this paper.

Data availability

Data will be made available on request.

Acknowledgements

The authors gratefully acknowledge the financial support provided to this study by the Ministry of Science and Technology of Taiwan, ROC, under Project No. MOST 110-2221-E-020-011.

References

[1] W. Hou, S.B. Cronin, A review of surface plasmon resonance-enhanced photocatalysis, Advanced Functional Materials 23 (13) (2013) 1612–1619.
[2] H.W. Chen, K.C. Hsu, Y.C. Chan, J.G. Duh, J.W. Lee, J.S.C. Jang, G.J. Chen, Antimicrobial properties of Zr–Cu–Al–Ag thin film metallic glass, Thin Solid Films 561 (2014) 98–101.
[3] Y.Y. Chu, Y.S. Lin, C.M. Chang, J.K. Liu, C.H. Chen, J.C. Huang, Promising antimicrobial capability of thin film metallic glasses, materials science & engineering C, Materials for biological applications 36 (2014) 221–225.
[4] Y.H. Lin, J.J. Wang, Y.T. Wang, H.K. Lin, Y.J. Lin, Antifungal properties of pure silver films with nanoparticles induced by pulsed-laser dewetting process, Applied Sciences 10 (7) (2020) 2260.
[5] J.J. Wang, H.K. Lin, W.S. Chuang, C.Y. Chuang, Y.H. Lin, J.C. Huang, Y.H. Lin, Laser dewetting mechanism and antibacterial properties of Cu-Al based medium entropy alloy films, Journal of Alloys and Compounds 903 (2022) 163893.
[6] H.K. Lin, T.-Y. Li, I.C. Chen, Y.C. Lo, Laser-induced surface plasmon resonance and SERS performance of AgCuAl medium entropy alloy films, Materials Letters 333 (2023) 133701.
[7] Y.J. Lin, H.K. Lin, Y.H. Lin, Construction of Raman spectroscopic fingerprints for the detection of Fusarium wilt of banana in taiwan, PLoS One 15 (3) (2020) e0230330.
[8] G. An, S. Li, W. Zhang, Z. Fan, Y. Bao, A polarization filter of gold-filled photonic crystal fiber with regular triangular and rectangular lattices, Optics Communications 331 (2014) 316–319.
[9] C. Noguez, Surface plasmons on metal nanoparticles: The influence of shape and physical environment, The Journal of Physical Chemistry C 111 (2007) 3806–3819.
[10] S.L.a.M.A. El-Sayed, Spectral properties and relaxation dynamics of surface plasmon electronic oscillations in gold and silver nanodots and nanorods, The Journal of Physical Chemistry B 103 (1999) 8410–8426.
[11] Y.Y. Liang, X. Lin, M. Liang, F.C. Brunicardi, P. ten Dijke, Z. Chen, K.W. Choi, X. H. Feng, dSmurf selectively degrades decapentaplegic-activated MAD, and its overexpression disrupts imaginal disc development, J Biol Chem 278 (29) (2003) 26307–26310.
[12] P. Ma, F. Liang, Y. Sun, Y. Jin, Y. Chen, X. Wang, H. Zhang, D. Gao, D. Song, Rapid determination of melamine in milk and milk powder by surface-enhanced Raman spectroscopy and using cyclodextrin-decorated silver nanoparticles, Microchimica Acta 180 (11–12) (2013) 1173–1180.
[13] A. Kumar, K.M. Gangawane, Synthesis and effect on the surface morphology & magnetic properties of ferrimagnetic nanoparticles by different wet chemical synthesis methods, Powder Technology 410 (2022) 117867.
[14] N. Suresh Kumar, R. Padma Suvarna, K. Chandra Babu Naidu, P.P. Mohapatra, P. Dobbidi,, X-band electromagnetic properties of hydrothermally synthesized La1-xBixTiO3 (x = 0.2–0.8) nanoparticles, Inorganic Chemistry Communications 149 (2023) 110408.
[15] H. Zheng, M.S. Matseke, T.S. Munonde, The unique Pd@Pt/C core-shell nanoparticles as methanol-tolerant catalysts using sonochemical synthesis, Ultrason Sonochem 57 (2019) 166–171.
[16] Y. Oh, M. Lee, Single-pulse transformation of Ag thin film into nanoparticles via laser-induced dewetting, Applied Surface Science 399 (2017) 555–564.
[17] Y. Oh, J. Lee, M. Lee, Fabrication of Ag-Au bimetallic nanoparticles by laser-induced dewetting of bilayer films, Applied Surface Science 434 (2018) 1293–1299.
[18] H.K. Lin, J.J. Wang, W.H. Lu, W.S. Chuang, C.Y. Chen, H.S. Chou, J.C. Huang, Microstructure and optical properties of AgCuAl medium entropy films with nanoparticles induced by pulsed-laser dewetting, Surface and Coatings Technology 421 (2021) 127427.
[19] N. Abid, A.M. Khan, S. Shujait, K. Chaudhary, M. Ikram, M. Imran, J. Haider, M. Khan, Q. Khan, M. Maqbool, Synthesis of nanomaterials using various top-down and bottom-up approaches, influencing factors, advantages, and disadvantages: A review, Advances in colloid and interface science 300 (2022) 102597.
[20] P. Pandey, S. Kunwar, J. Lee, Solid state dewetting of Ag/Pt bilayers for the stronger localized surface plasmon resonance (LSPR) properties: The dynamic control of surface morphology and elemental composition of AgPt and Pt nanostructures by the auxiliary Ag layer, Journal of Alloys and Compounds 813 (2020) 152193.
[21] A. Le Bris, F. Maloum, J. Teisseire, F. Sorin, Self-organized ordered silver nanoparticle arrays obtained by solid state dewetting, Applied Physics Letters 105 (20) (2014).
[22] D. Wang, P. Schaaf, Solid-state dewetting for fabrication of metallic nanoparticles and influences of nanostructured substrates and dealloying, physica status solidi (a) 210 (2013) 1544–1551.
[23] P.D. Rack, Y. Guan, J.D. Fowlkes, A.V. Melechko, M.L. Simpson, Pulsed laser dewetting of patterned thin metal films: A means of directed assembly, Applied Physics Letters 92 (22) (2008) 223108.
[24] S. Yang, F. Xu, S. Ostendorp, G. Wilde, H. Zhao, Y. Lei, Template-confined dewetting process to surface nanopatterns: Fabrication, structural tunability, and structure-related properties, Advanced Functional Materials 21 (13) (2011) 2446–2455.
[25] F. Ruffino, A. Gentile, M. Zimbone, G. Piccitto, R. Reitano, M.G. Grimaldi, Size-selected Au nanoparticles on FTO substrate: Controlled synthesis by the rayleigh-taylor instability and optical properties, Superlattices and Microstructures 100 (2016) 418–430.
[26] Y. Kazakova, Y. Andreeva, M. Sergeev, V. Mikhailovskii, E. Ageev, Formation of nanoparticles from thin silver films under a liquid layer by single-shot nanosecond laser action, Optical and Quantum Electronics 52 (2) (2020) 97.
[27] S. Yadavali, R. Kalyanaraman, Nanomaterials synthesis by a novel phenomenon: The nanoscale rayleigh-taylor instability, AIP Advances 4 (4) (2014) 047116.
[28] E.I. Ageev, I.R. Aminov, M.A. Baranov, Y.D. Golubev, G.V. Odintsova, P. V. Varlamov, Evolution of thin silver films under exposure to laser pulses in the air, Optical and Quantum Electronics 49 (2) (2017) 56.
[29] J. Bosbach, D. Martin, F. Stietz, T. Wenzel, F. Träger, Laser-based method for fabricating monodisperse metallic nanoparticles, Applied Physics Letters 74 (18) (1999) 2605–2607.
[30] R.G. Nikov, N.N. Nedyalkov, P.A. Atanasov, D. Hirsch, B. Rauschenbach, K. Grochowska, G. Sliwinski, Characterization of Ag nanostructures fabricated by laser-induced dewetting of thin films, Applied Surface Science 374 (2016) 36–41.
[31] H. Oh, J. Lee, M. Seo, I.U. Baek, J.Y. Byun, M. Lee, Laser-induced dewetting of metal thin films for template-free plasmonic color printing, ACS Applied Materials & Interfaces 10 (44) (2018) 38368–38375.
[32] S. Yadavali, M. Khenner, R. Kalyanaraman, Pulsed laser dewetting of Au films: Experiments and modeling of nanoscale behavior, Journal of Materials Research 28 (13) (2013) 1715–1723.
[33] M. Kawasaki, M. Hori, Laser-induced conversion of noble metal-island films to dense monolayers of spherical nanoparticles, The Journal of Physical Chemistry B 107 (28) (2003) 6760–6765.
[34] H. Krishna, N. Shirato, C. Favazza, R. Kalyanaraman, Pulsed laser induced self-organization by dewetting of metallic films, Journal of Materials Research 26 (2) (2011) 154–169.

[35] D.D. Evanoff Jr., G. Chumanov, Synthesis and optical properties of silver nanoparticles and arrays, Chemphyschem 6 (7) (2005) 1221–1231.
[36] X. Liu, D. Li, X. Sun, Z. Li, H. Song, H. Jiang, Y. Chen, Tunable dipole surface plasmon resonances of silver nanoparticles by cladding dielectric layers, Sci Rep 5 (2015) 12555.
[37] H.K. Lin, Y.T. Wang, W.S. Chuang, H.S. Chou, J.C. Huang, Surface resonance properties of pure Cu and Cu80Zr20 metallic glass films with nanoparticles induced by pulsed-laser dewetting process, Applied Surface Science 507 (2020) 145185.
[38] J. Wang, Y. Hu, X. Yu, X. Zhuang, Q. Wang, N. Jiang, J. Hu, Recyclable and ultrasensitive SERS sensing platform: Deposition of atomically precise Ag152 nanoclusters on surface of plasmonic 3D ZnO-NC/AuNP arrays, Applied Surface Science 540 (2021) 148324.
[39] M.A. Basyooni, A.M. Ahmed, M. Shaban, Plasmonic hybridization between two metallic nanorods, Optik 172 (2018) 1069–1078.
[40] X. Xue, L. Lu, D. He, Y. Guan, Y. Li, Antibacterial properties and cytocompatibility of Ti-20Zr-10Nb-4Ta alloy surface with Ag microparticles by laser treatment, Surface and Coatings Technology 425 (2021) 127716.
[41] S. Rajagopalachar, J. Pattar, S. Mulla, Synthesis and characterization of plate like high surface area MgO nanoparticles for their antibacterial activity against bacillus cereus (MTCC 430) and pseudomonas aeruginosa (MTCC 424) bacterias, Inorganic Chemistry Communications 144 (2022) 109907.
[42] C. Marambio-Jones, E.M.V. Hoek, A review of the antibacterial effects of silver nanomaterials and potential implications for human health and the environment, Journal of Nanoparticle Research 12 (5) (2010) 1531–1551.
[43] C. Baker, A. Pradhan, L. Pakstis, D.J. Pochan, S.I. Shah, Synthesis and antibacterial properties of silver nanoparticles, J Nanosci Nanotechnol 5 (2) (2005) 244–249.
[44] J. Ye, B. Li, M. Li, Y. Zheng, S. Wu, Y. Han, ROS induced bactericidal activity of amorphous Zn-doped titanium oxide coatings and enhanced osseointegration in bacteria-infected rat tibias, Acta Biomater 107 (2020) 313–324.
[45] A. Herman, A.P. Herman, Nanoparticles as antimicrobial agents: Their toxicity and mechanisms of action, J Nanosci Nanotechnol 14 (1) (2014) 946–957.